Available online at www.sciencedirect.com

ScienceDirect

journal homepage: http://www.elsevier.com/locate/acme

Original Research Article

Localizing impact damage of composite structures with modified RAPID algorithm and non-circular PZT arrays

Michał Dziendzikowski [a], *Krzysztof Dragan* [a], *Andrzej Katunin* [b,*]

[a] *Air Force Institute of Technology, 6 Ks. Boleslawa Street, 01-494 Warsaw, Poland*
[b] *Institute of Fundamentals of Machinery Design, Silesian University of Technology, 18A Konarskiego Street, 44-100 Gliwice, Poland*

ARTICLE INFO

Article history:
Received 17 May 2016
Accepted 26 September 2016
Available online 20 October 2016

Keywords:
Structural health monitoring
Guided waves damage localization
Vibration-based impact damage localization
Barely visible impact damage

ABSTRACT

Detecting and localizing impact damage of composite structures is one of the key expectations towards development of structural health monitoring (SHM) systems. In this paper, a method intended to meet these requirements is presented. The developed method is based on guided waves actuation in a monitored structure. One of the methods used for damage localization with guided waves is the RAPID/PRA algorithm. This algorithm is mostly used for circular arrays of PZT piezoelectric transducers. In the paper a modification of this approach, adopted to be used for more general geometries of PZT networks is presented. Its main improvement is that predicted location of damage is less biased by inhomogeneous distributions of sensing paths, i.e. lines connecting pairs of transducers of a network, than for RAPID algorithm. The developed method was verified experimentally on composite laminated specimens with introduced damage caused by low energy impact. Detailed description of the developed algorithm as well as the results of impact damage localization tests are delivered in the paper.

1. Introduction

One of the major issues which could increase safety of aircraft operation is the automated early detection of different damage modes of composite structures [1,2]. Composites are vulnerable to impacts, even of low energies, which can introduce in the structure the so called barely visible impact damage (BVID) [3]. BVID can decrease the stiffness and durability of a composite due to multiple delaminations and transverse cracks of its layers (Fig. 1) [4,5].

The most commonly used non-destructive technique for BVID detection and localization is the ultrasonic testing (UT). This technique allows for precise damage localization and sizing [6], however its application is possible during the ground aircraft maintenance. Furthermore, random nature of BVID occurrence introduces additional risk factor, which needs to be considered in aircraft design approaches. In particular,

* *Corresponding author.*
E-mail address: andrzej.katunin@polsl.pl (A. Katunin).
http://dx.doi.org/10.1016/j.acme.2016.09.005
1644-9665/

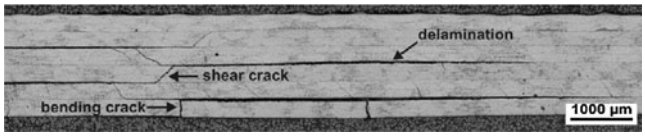

Fig. 1 – An example of BVID of composite structure [5].

estimated time intervals between NDT inspections are burdened with additional uncertainty, which can jeopardize the safety. Therefore, development of structural health monitoring (SHM) systems that allow for continuous structure assessment, e.g. BVID detection, is one of the key technology demanded by the aerospace industry [7].

One of the approaches to detect BVID and other damage of composite structures is to use networks of PZT transducers actuating elastic waves in a monitored element [8–11]. Due to the complexity of signals, which are acquired over a long acquisition time compared to classical UT method, the condition of a monitored structure is assessed with use of baselines, i.e. signals obtained for the initial state of the structure. For evaluation of changes of baselines caused by damage, e.g. BVID, numerical signal characteristics called the damage indices (DIs) are often used [11]. DIs can be used also for the purpose of damage localization, e.g. as in RAPID/PRA algorithm [12–15].

The RAPID method is based on a weighted sum of functions that represent geometry of sensing paths, i.e. lines joining pairs of PZT transducers, with weights in the form of a DI obtained for each pair of sensors. Assuming that sensing paths are homogeneously distributed in the monitored region, damage can be localized using this algorithm. However, if the geometry of the network contains points where sensing paths are focused the damage localization map obtained with RAPID algorithm can be heavily distorted towards such points.

In this paper, a modification of RAPID algorithm is presented. The performance of damage localization for non-circular PZT arrays is improved with respect to RAPID method. The approach was verified experimentally by localizing BVID of composite specimens. Applied PZT networks were composed of two parallel linear arrays. As shown, for such network geometry, localization of BVID with RAPID algorithm is heavily biased towards the network's center. BVID localization is significantly improved by the proposed modification. The results were verified using ultrasonic tests as well as wavelet-based analysis of modal shapes. The proposed modification of the RAPID algorithm makes possible detection and precise localization of structural damage, in particular BVID, due to the lowering of an influence of topology of PZT transducers placement.

2. Modified RAPID algorithm

In general, there exist two approaches for localizing damage within a given sensor network: one utilizes the entire information carried by signals, and the other one is based on the DIs as the RAPID algorithm. Both of them have their own advantages and limitations which will be briefly discussed below.

The general idea of approaches based on full signal waveforms [14,16–18] can be explained on the following simplified example. Let f_{gs} denotes a signal obtained for a generator g and a sensor s and $f_{gs,b}$ denotes the corresponding baseline. Then, for a given sensing path $g \rightarrow s$ and a point p of the monitored area, the so called partial damage intensity map $I_{gs}(p)$, indicating the most probable damage locations, can be defined as:

$$I_{gs}(p) = \left| f_{gs}(t_{gp} + t_{ps}) - f_{gs,b}(t_{gp} + t_{ps}) \right|, \tag{1}$$

where t_{gp} is the time needed to reach point p by an elastic wave actuated by the generator g, and t_{ps} is the time after which the wave eventually scattered at the point p is received by the sensor s. When considering homogeneous and isotropic medium, the above expression can be rewritten as:

$$I_{gs}(p) = \left| f_{gs}\left(\frac{l_{gp} + l_{sp}}{c}\right) - f_{gs,b}\left(\frac{l_{gp} + l_{sp}}{c}\right) \right|, \tag{2}$$

where l_{gp}, l_{sp} denotes the distance of the point p from the generator g or the sensor s, respectively, and c is the propagation speed of a given elastic wave mode. In this case, partial damage intensity is constant on the ellipses having focal points in the location of the transducers forming a given sensing path. The partial intensity map I_{gs} obtained for a given sensing path indicate regions, where damage should be located in order to distort the signal at time instances where the highest differences are present. The information from all of the network sensing paths can be merged in the so called total damage intensity map I defined either as the sum:

$$I(p) = \sum_{g \rightarrow s} I_{gs}(p) \tag{3}$$

or the product:

$$I(p) = \prod_{g \rightarrow s} I_{gs}(p) \tag{4}$$

of partial intensity maps I_{gs}, which is known as the delay-sum or delay-multiply procedure [14].

The alternative approaches to localize damage, e.g. the RAPID algorithm [12–15], utilize the following observation. Due to the energy conservation principle, elastic waves scattered on local damage of a structure are vanishing with the distance from it. Thus, eventual contributions to signal due to damage presence, are the most visible for sensing paths running close to a damage. Therefore, in order to visualize it one can introduce partial intensity map of the form:

$$I_{gs}(p) = DI(g, s) R_{gs}(p), \tag{5}$$

where $DI(g, s)$ is a given damage index, i.e. some numerical signal characteristics [11], and R_{gs} is a function representing an effective range of a given sensing path $g \rightarrow s$ (Fig. 2).

For a given point p the function R_{gs} weights the intensity of the influence of a possible damage located at p on the signal obtained for this sensing path, thus R should decrease when the distance from it increases. Again, as in the previous approach the joint information from a network of PZT sensors can be utilized either as the sum (3) or the product (4) of partial

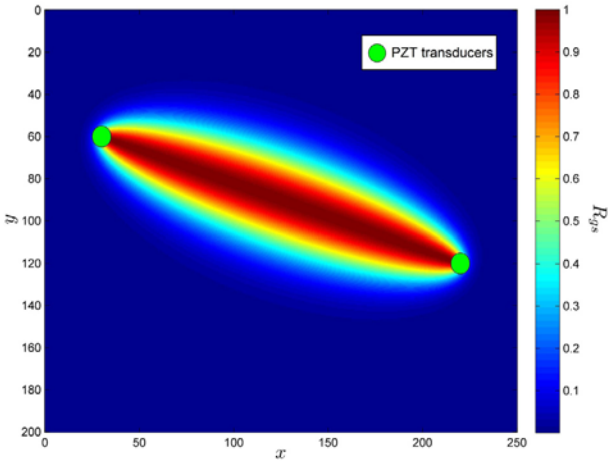

Fig. 2 – An example of a sensing path effective range R_{gs}.

intensity maps (5). Indeed, the intensity map of the RAPID algorithm reads as follows:

$$I_{\mathrm{RAPID}}(p) = \sum_{g \to s} DI(g,s) R_{gs}, \tag{6}$$

where $DI(g, s)$ is based on correlation of signal with its corresponding baseline and up to a constant

$$R_{gs}(p) = \frac{1}{2} \begin{cases} \beta - \dfrac{l_{gp} + l_{sp}}{l_{gs}}, & \dfrac{l_{gp} + l_{sp}}{l_{gs}} < \beta, \quad \beta > 1, \\ 0, & \dfrac{l_{gp} + l_{sp}}{l_{gs}} \geq \beta, \end{cases} \tag{7}$$

with the notation kept as in (2). The cutting parameter β restricts the support of the function R_{gs} in order to remain a proper resolution of the algorithm, usually $\beta \approx 1.05$ [12,13].

The RAPID algorithm allows for localization of damage and their size estimation. Since it utilizes much less information carried by the signal than the approaches rooted in Eq. (1), it is usually less influenced by signal distortions caused by non-damage related factors. In fact, all of such effects contribute to values of DI's used in (5), but sensing paths geometries R_{gs} remain unchanged. Signal disturbances, e.g. elevated noise level, can results in apparent damage loci for I_{gs} of the form based on Eq. (1).

However, in order to obtain the satisfactory results, RAPID algorithm usually needs more transducers than in the case of the full information approach. Furthermore, its capabilities depend heavily on the geometry of an applied PZT network. For circular networks, for which RAPID is mostly used, sensing paths and their intersections are rather homogeneously distributed (Fig. 3(a)), thus damage can be faithfully visualized irrespectively of its location within the network. For different geometry of PZT network, visualization of damage of the same size may depend on their location [13]. As an example one can consider parallel PZT network for which damage located at different points, e.g. A, B, C in Fig. 3(b) is distorted along axis perpendicular to the network direction, due to inhomogeneities in distribution of sensing paths intersections (Fig. 3(b)).

In this paper yet another issue related to the network geometry is addressed. For RAPID algorithm the estimated location of damage is shifted towards focal points of the network, i.e. points at which number of intersecting sensing paths is higher than at other locations. For indication of regions, where sensing paths are concentrated, the signature function of a network geometry:

$$N(p) = \sum_{g \to s} R_{gs}(p) \tag{8}$$

can be used. Signatures, calculated for two different networks when assuming that

$$R_{gs}(p) = \left(\frac{l_{gs}}{l_{gp} + l_{sp}} \right)^{\alpha}, \quad \alpha = 40, \tag{9}$$

are presented in Fig. 4.

Signature function N is rather homogeneous for the network of circular topology (Fig. 4(a)), whereas for the parallel geometry of the network its center is clearly distinguished as a focal point (Fig. 4(b)).

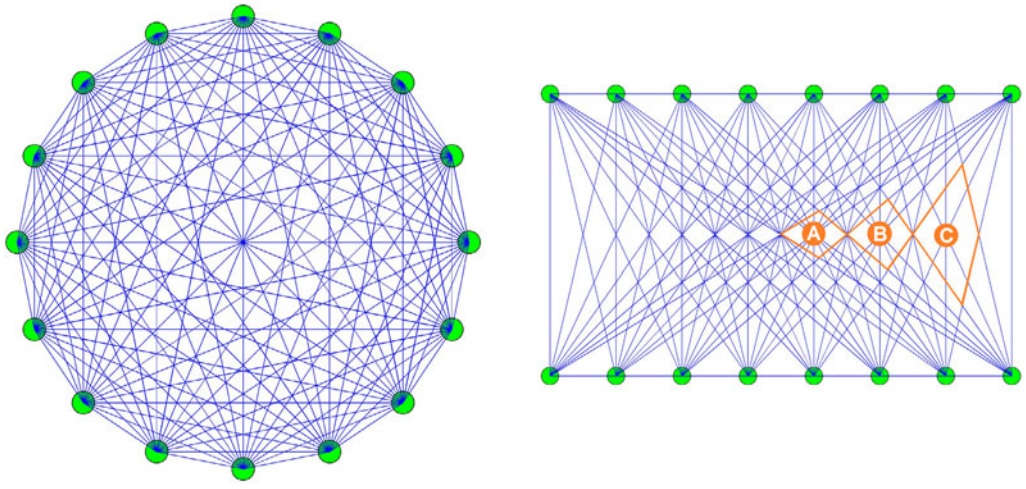

(a) circular geometry (b) parallel geometry

Fig. 3 – Examples of PZT network geometries.

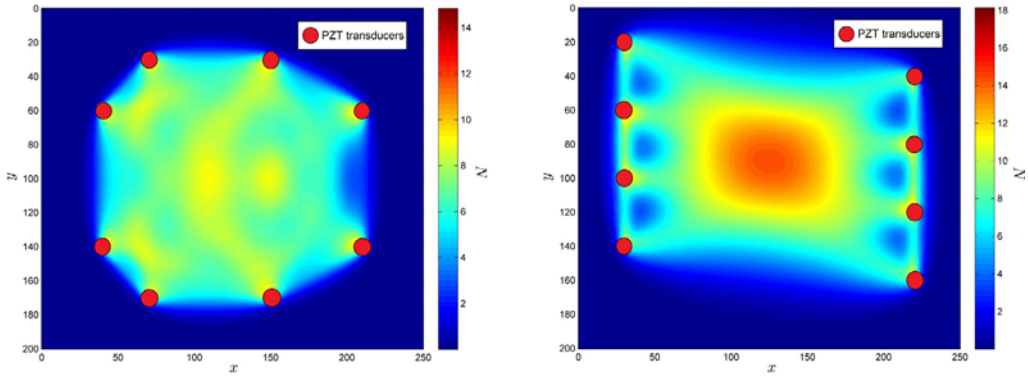

Fig. 4 – Examples of normalization factor N for different network geometries.

In principle, this should not be an issue since in the formula (6), sensing paths R_{gs} are weighted with values of DIs obtained for them, which for sensing paths distant from a damage should be equal to zero. In practice DIs on any sensing path is different than zero due to signal distortions caused by factors other than damage, e.g. signal noise. If the signature N of a network is homogeneous (Fig. 4(a)), this is not an issue assuming all sensing paths are similarly influenced by non-damage factors. However, if focal points exist within the network, as for example in Fig. 4(b), the value of intensity map I_{RAPID} (6) is artificially increased in the vicinity of a focal point, resulting in bias of damage localization.

In order to improve damage localization precision, the network signature function can be used as a normalizing factor in the intensity map:

$$I_N(p) = \frac{1}{N(p)} \sum_{g \to s} DI(g,s) R_{gs}(p). \tag{10}$$

For normalized intensity map, focal points has less influence on estimated damage localization, but still shape distortions of damage visualization can appear for networks with inhomogeneously distributed points of sensing paths intersections (Fig. 3(b)). Note that such normalization is possible only if N has well defined reciprocal, thus R_{gs} of the form (7), used in original RAPID algorithm, cannot be applied for normalized intensity map. However, also the non-vanishing fast decaying function can be used to represent effective range R_{gs} of sensing paths. An example of such function is given by (9). Effectively, its support is restricted to bounded area around the segment connecting two transducers. Using the parameter α it can be tuned to represent sensing paths as in (7), thus it can be used as its alternative.

3. Localizing BVID damage with modified RAPID algorithm

In order to verify the proposed BVID localization method (10) a test structure was manufactured in the form of glass fiber-reinforced plastic (GFRP) using the prepreg technology with Heatcon control unit and heating blanket. Unidirectional glass/epoxy prepreg tape was used and the stacking sequence of the layers was $[0/45/-45/0]_S$. In order to verify an effectiveness of the two proposed approaches the low-velocity impact drop tests were performed on the GFRP specimen in order to introduce BVID in various locations. On the surface of the specimen a parallel network of PZT transducers was deployed. Applied transducers were manufactured in the form of multilayered PZT plates by Noliac A/S with a thickness of 2 mm and an edge length of 3 mm. The multiple low-velocity impact damage sites were introduced in the structure in three locations by dropping impactor with the energy of 9, 6 and 3 J, subsequently. The characteristic dimensions, locations of PZT sensors, as well as introduced impact damage sites of the tested structure are presented in Fig. 5. Impacts were performed by dropping an axially symmetric impactor from different heights corresponding to the assumed energies.

3.1. *Ultrasonic damage identification*

The impacts caused BVID in the specimen whose extent, measured by ultrasonic technique (Fig. 6), depended on the energy of impact. For the ultrasonic inspection the automated

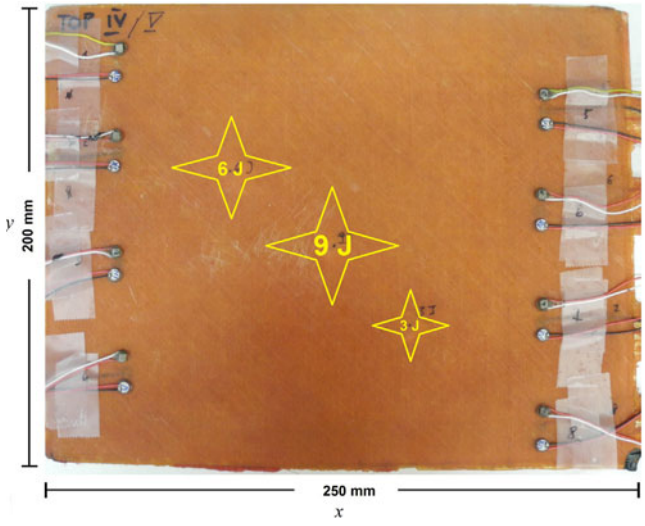

Fig. 5 – The GFRP specimen with attached PZT transducers and location of impact damage.

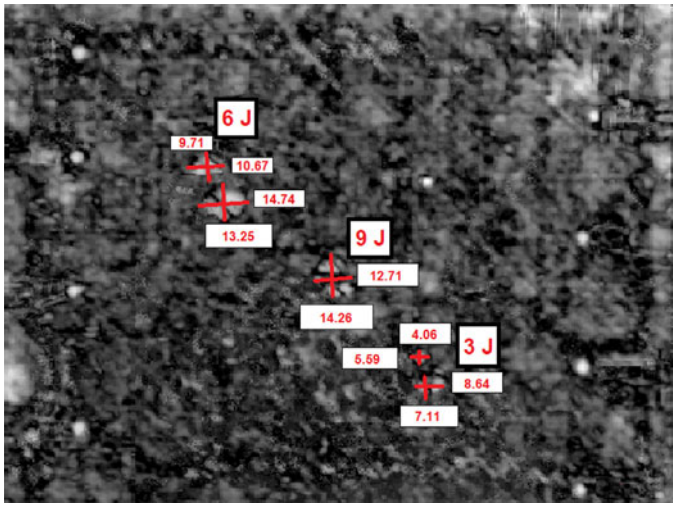

Fig. 6 – Ultrasonic C-Scan of the GFRP specimen (BVID dimensions given in millimeters).

MAUS® system of the Boeing company was used. The system enables capturing of ultrasonic data (time of flight (ToF) and amplitude peak location) based on selected signal gates. The results of the inspection can be visualized in the form of C-scan mapping (Fig. 6) representing a chosen signal feature with respect to the position of ultrasonic probe. In this case, a peak-to-peak value of a signal resulted from the reflection from the bottom part of the specimen was selected. On this the basis damage can be identified and characterized.

The dimensions of the 9 and the 6 J BVID in the acquired C-scan map are comparable (see Fig. 6), which is resulted due to possible rotation of the impactor after its releasing from a given height. The 3 J impact damage is considerably smaller than the other ones.

3.2. *Wavelet-based analysis of modal shapes*

As an additional verification, another NDT method was applied. The tested specimen with BVID was inspected using vibration-based method with further processing of modal shapes by the wavelet transform which allows detecting and localizing BVID in the tested structure. The wavelet transform of modal shapes allows identifying singularities in modal response data resulting from a local decrease of stiffness of the tested structures.

The acquisition of modal shapes of vibration of the tested structure was performed as a classical modal analysis. The tested specimen was clamped in the steel frame on two opposite edges (the other two edges remained free). The frame with the specimen was mounted on the electrodynamic shaker TIRA® TV-51120. The tested structure was excited by pseudo-random noise signal amplified by the power amplifier TIRA® BAA 500 connected with the shaker. Two laser Doppler vibrometers (LDVs) were used during the measurement procedure: the scanning LDV Polytec® PSV-400 was used for the measurement of velocity of displacements in the net of measurement points defined on the surface of the plate, while the point LDV Polytec® PDV-100 was focused on the clamping frame and used for obtaining the reference signal. In order to enhance the quality of measured signals the specimen was covered by the Helling® anti-glare spray before the scanning. The experimental setup is presented in Fig. 7.

Due to the clamping of the specimen the scanning area was limited to 254 mm × 205 mm. Accordingly, the net of measurement points on the resulting scanning area was defined as 79 × 61 points. The parameters of the experiment were as follows. The testing frequency bandwidth was set to 0–1.6 kHz with a resolution of 1 Hz with five cycles of averaging of measured values of velocity of vibration in each defined measurement point.

Considering that the locations of BVID sites were a priori known and a fact that the magnitude of velocity of vibration of the first modal shape is high enough in the locations of BVID (which is directly connected with effectiveness of further

Fig. 7 – Experimental setup of vibration-based non-destructive tests.

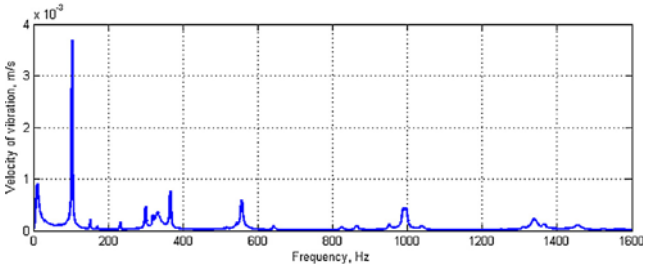

Fig. 8 – FRFs of the tested specimen.

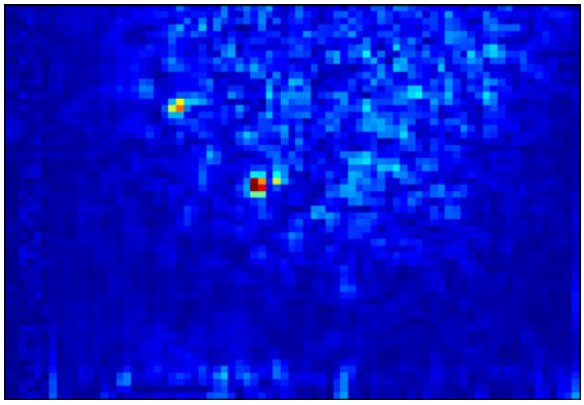

Fig. 9 – Results of vibration-based damage identification.

applied wavelet-based processing), it was decided to consider only the first modal shape. The next two excited modal shapes have the magnitudes of velocity of vibration of 4.8 and 6.2 times lower (see the frequency response functions (FRFs) shown in Fig. 8).

The acquired modal shape was analyzed using the single-level 2D undecimated discrete wavelet transform (UDWT), which, in spite of its redundancy with respect to its decimated version, does not cause the resolution reduction and is characterized by better shift invariance. The B-spline wavelet of order 3 was selected for the analysis. The decomposition using UDWT resulted in the set of approximation coefficients and three directional sets of detail coefficients. Since the detail coefficients consisted of the information on detected singularities in modal shapes in specific directions (horizontal, vertical and diagonal) they were considered in further processing.

In order to identify the damage locations and shapes of damaged regions it was essential to add up the absolute values of the mentioned sets. The resulted set of coefficients obtained after described processing procedure is presented in Fig. 9.

Two damaged regions are well detectable (impacts of 6 and 9 J) in Fig. 9, similarly as in the case of ultrasonic tests, while the 3 J impact damage was not detected.

3.3. *BVID localization with PZT network*

Before the test and after each of the subsequent impacts of the energy 9, 6 and 3 J, series of measurements were performed for the deployed PZT network. The measurements were arranged in the pitch-catch configuration, obtaining the signal for each pair of the transducers, i.e. a sensing path. The excitation signal of PZT transducers was Hanning windowed with 8 periods of duration at the frequency of 150 kHz. For the measurements the data acquisition unit PAQ16000D manufactured by EC Electronics, Poland, was used.

Damage index used in intensity maps (6), (10) was based on the correlation coefficient $r_{f_{gs}^{env} f_{gs,b}^{env}}$ of the envelope f_{gs}^{env} of a signal obtained for the generator g and the sensor s with the envelope of the corresponding baseline $f_{gs,b}^{env}$, i.e. the signal obtained for the initial (not necessarily undamaged) state of the structure:

$$DI(g,s) = 1 - r_{f_{gs}^{env} f_{gs,b}^{env}}. \tag{11}$$

The baseline signals were updated after each impact. For representation of sensing paths the function (9) was used. For that choice, the network signature function is presented in Fig. 4(b).

In Fig. 10, both the normalized (10) and RAPID (6) intensity maps are presented.

The determined location of impact damage are defined as points at which maximum value of intensity map, i.e. I_{RAPID} or I_N, is attained. Intensity maps (Fig. 10(a), (c) and (e)) obtained with use of RAPID algorithm are heavily influenced by the network geometry. The determined location of impact damage is moved towards the specimen center, where most of the sensing paths intersect (Fig. 4(b)). Indeed, all of the determined impact damage locations are very close to this point and they almost do not change for different impacts. The determined locations of impact damage using normalized intensity function I_N (10) are in better agreement with the actual impact positions (Fig. 10(b), (d) and (f)). As expected, normalized intensity maps are distorted in the direction perpendicular to the two lines of transducers (Fig. 5). The algorithm resolution along this direction can be greatly improved by introducing additional transducers which would make the shape of the network more circular-like.

4. Verification of the modified imaging method on a test aircraft structure

The modification of RAPID damage localization algorithm in a way that it is suitable to be used for non-homogeneous networks was also driven by some technical considerations. For composites, besides the possibility of the transducers attachment to the surface of a tested element, embedding of PZT transducers into their internal structure is also possible [19–22]. Certainly, the most straightforward method of integration is to bind the transducers with the surface, whereas the embedding poses several issues. The most important is their influence on the mechanical properties of the host structure. The embedded transducers can change locally the stiffness of a composite as well as decrease its tensile and fatigue strength [21,23]. Embedding of sensors should be performed during manufacturing process of a composite structure, which makes it more complicated, and thus, more expensive [11].

However, transducers embedding can be desired in some cases. One of them is when considering repairs of the structure

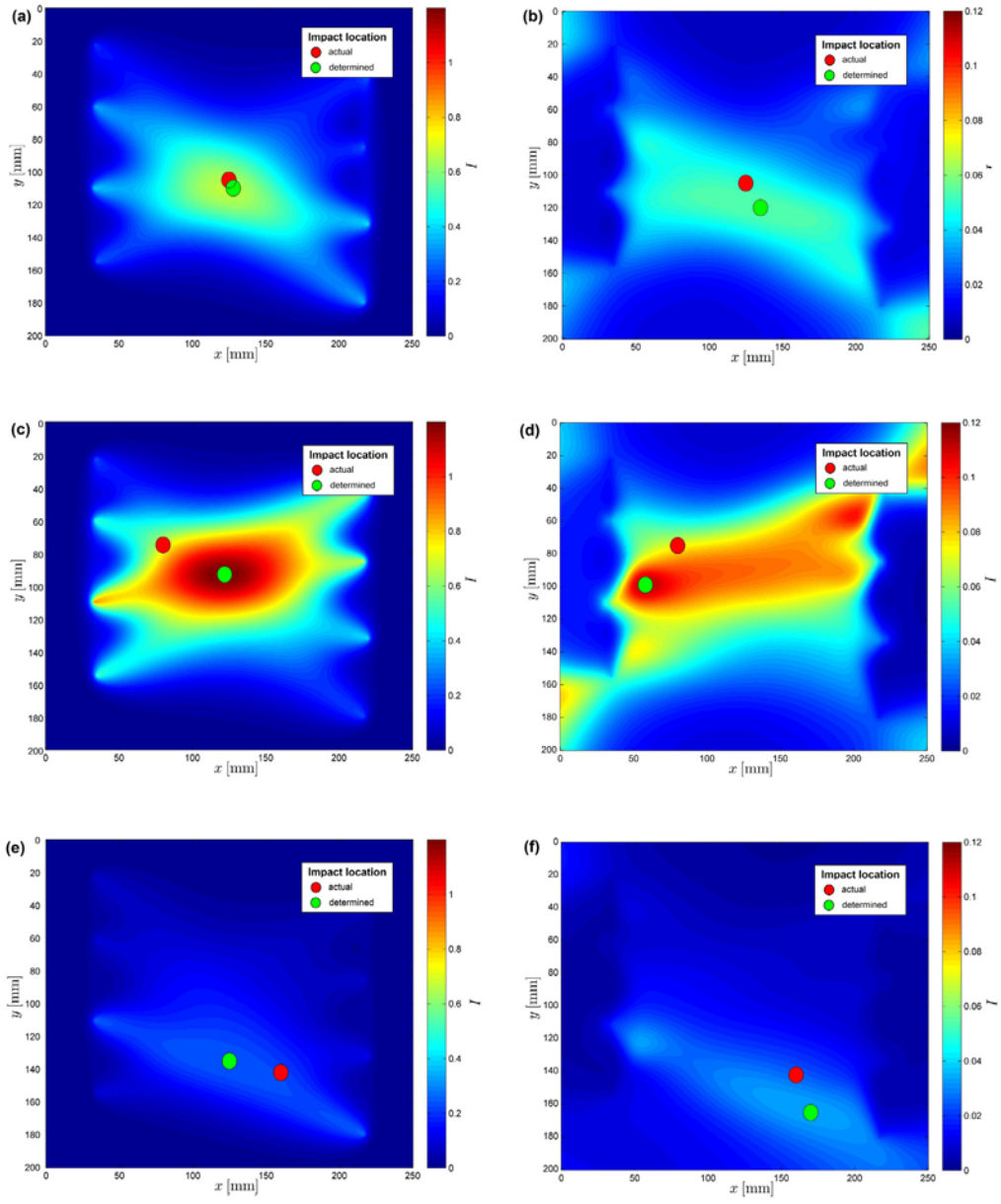

Fig. 10 – Intensity functions (6), (10) for BVID localization: (a) I_{RAPID} after 9 J impact, (b) I_N after 9 J impact, (c) I_{RAPID} after 6 J impact, (d) I_N after 6 J impact, (e) I_{RAPID} after 3 J impact, (f) I_N after 3 J impact

by composite patches [24,25]. For repairs of the outer structures it may happen that the only way to use PZT transducers is to embed them into the patches, since otherwise they would be directly exposed to external environmental conditions. The other case is related to increasing damage detection capabilities of the approach. The acoustic coupling of the embedded transducers with the ambient medium is very strong, resulting in the better quality of the acquired signals. The embedded transducers are also less exposed to environmental conditions which delays their aging and makes the system more stable in the long term. However, the most important potential advantage of such an integration technique is the monitoring of multi-layer structures, e.g. fiber metal laminates (FML) [26] or

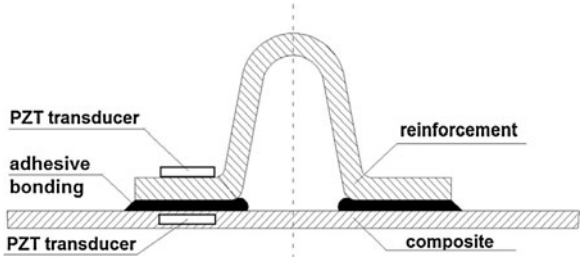

Fig. 11 – Possible configuration of PZT transducers for adhesive bondings monitoring.

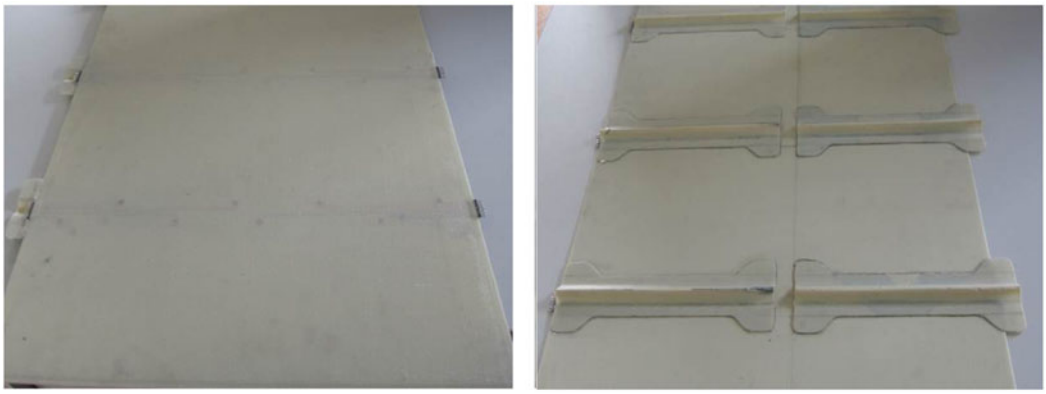

(a) top side (b) bottom side

Fig. 12 – GFRP test specimen with embedded PZT transducers

adhesive bondings (Fig. 11). Considering the possibility of embedding transducers between various layers of the structure, it opens a perspective to distinguish between inner layers delamination and debondings between layers made of different materials.

Therefore, networks with non-homogeneous geometry can be useful when considering the transducers embedding into the internal structure of a composite. Since the embedded transducers can locally change the stiffness as well as tensile and fatigue strength [21,23] of a host structure, the best location for the transducers is in the location of stiffeners of a structure.

In order to verify the proposed BVID localization method (10) for embedded PZT transducers, a test specimen with above described properties was manufactured (Fig. 12).

The specimen was made of GFRP composite with a set of reinforcement ribs attached to its surface. The network of 32 PZT transducers was embedded into the internal structure of

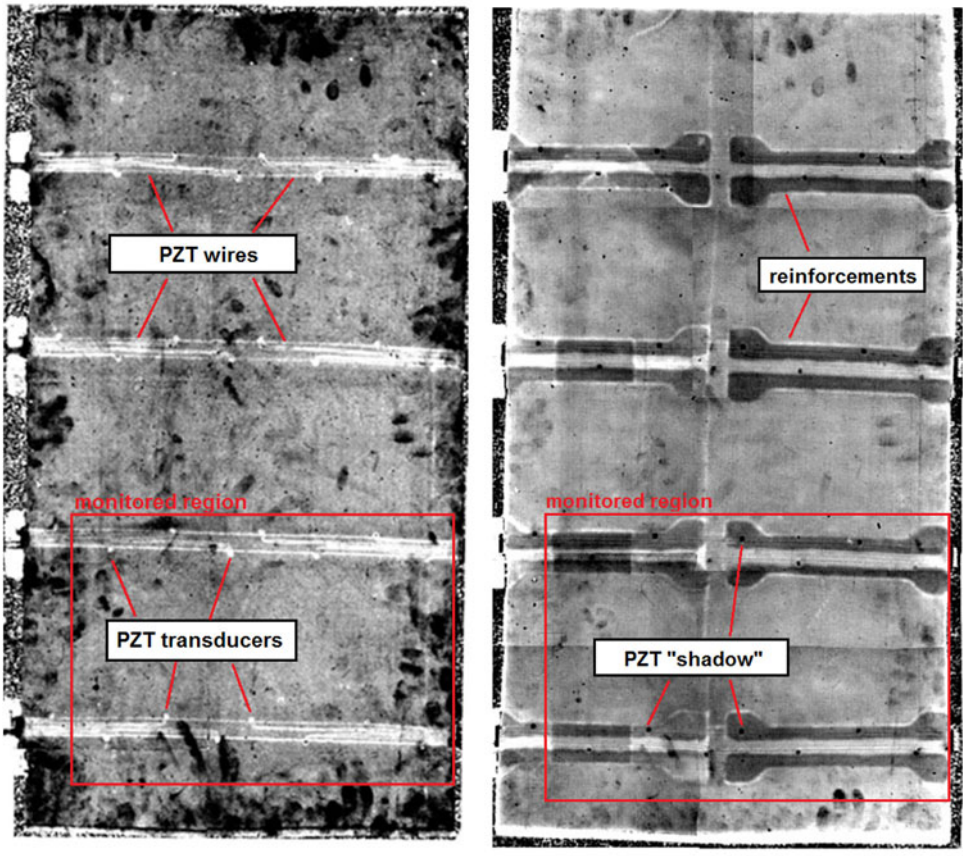

(a) 0.3 s after heating (b) 1.5 s after heating

Fig. 13 – Thermograms of the GFRP test specimen.

the specimen. The transducers were deployed during the manufacturing process in the middle plane of the specimen. PZT discs (with the code SMD05T04R111) made by STEMINC Inc. were used. Their diameter was of 5 mm and the thickness of 0.4 mm. The transducers were arranged to form a set of six parallel lines under the attached reinforcement ribs (see Figs. 11 and 12).

In Fig. 13 the results of the pulsed thermography inspection of the specimen are presented. For the purpose of the inspection the Echo Therm System of the Thermal Wave Imaging company with FLIR SC 7000 IR camera was used with the following setup:

- IR camera operation frequency – 54.71 Hz;
- Camera resolution – 320 × 240 pixels;
- Excitation Energy – 5 kJ;
- Wavelength – 1–5 μm;
- Time of thermal excitation – 4 ms;
- Time window for thermograms acquisition – 5 s.

The surface exposed to heat excitation is shown in Fig. 12(a).

Depending on the time after the specimen exposure on the heat impulse it is possible to visualize different cross sections of the specimen. Thermogram in Fig. 13(a), acquired 0.3 s after thermal excitation of the structure reveals details of the embedded network: the transducers location and power supply wires. In the other thermogram registered later (Fig. 13(b)), it is possible to distinguish clearly reinforcement's bonding and location of PZT transducers. The transducers obstructed the heat transfer to the bottom part of the specimen, thus, their shadow is visible in this thermogram.

Similarly, as in the previous case, the 9 J impact was performed by dropping an impactor on the specimen. Before and after the test, the impact measurements were performed for the PZT network using the same equipment as described previously. The signal exciting PZT transducers was Hanning windowed with 8 periods of duration and the frequency was set to 250 kHz. During this experiment a subnetwork of 14 PZT transducers closest to the impact location was used. The signature function of this subnetwork and the location of the transducers in the monitored frame is shown in Fig. 14. The center of the network is clearly distinguished.

The damage intensity maps I_{RAPID} (6) and I_N (10) for the introduced BVID are shown in Fig. 15. The resolution of damage location along the y-axis is poor for both algorithms. However, the normalized map is more precise along the x-axis of the specimen.

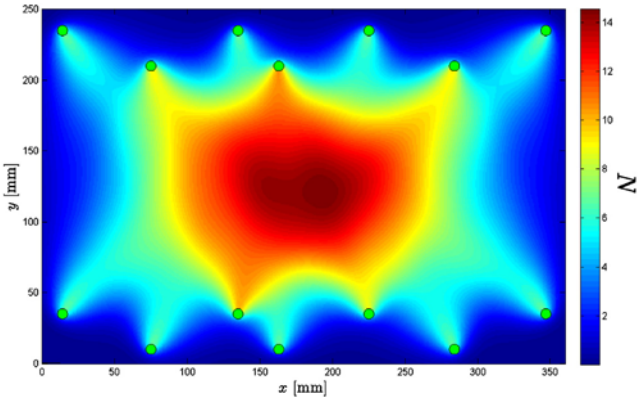

Fig. 14 – The signature function N for the subnetwork of the GFRP specimen used for the tests.

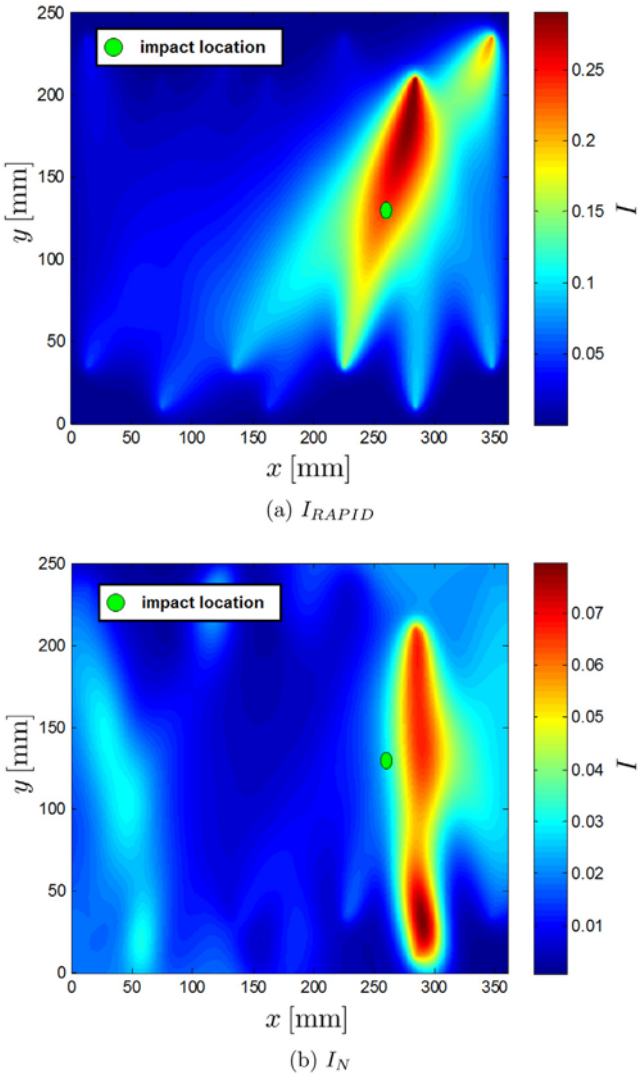

Fig. 15 – Intensity maps after impact.

5. Conclusions

In the paper, the approach to BVID monitoring based on network of active PZT transducers and modal analysis is presented. The proposed methods were verified based on impact tests of composite specimens. Modified RAPID imaging algorithm was able to localize BVID of the structure. The main advantage of the proposed approach is that it is less biased by the geometry of the transducers network than the original RAPID method. The introduced normalization factor improves the resolution of PZT networks composed by parallel linear arrays, but only along the direction of the arrays. In order to obtain better resolution in the direction perpendicular to the presented network, the introduction of additional PZT transducers is needed. In this case, the network geometry

becomes more homogeneous for which both the original and modified algorithms are equivalent.

The results were compared with other NDT techniques in order to verify damage presence and damage extent in the tested structures. The main goal of these studies was to obtain knowledge for further research in order to merge the two presented methods of BVID localization. This can be achieved by exciting natural frequencies of the specimen by PZT sensors and further data analysis based on specially designed time domain algorithms for modal shape analysis and linear fusion of the data from the selected sensors. This approach seems to be fast and efficient to use on real aerospace structures which will be an object of further investigations.

The proposed approach is going to be used for the composite structure of the remotely piloted aerial system (RPAS). The ultimate goal is to deliver fast and reliable inspection technique of such structures indicating roughly the location of damage. Due to the considerably high loads affecting such structures during take-off, maneuvers and landing and high risk of BVID occurrence a system of autonomous inspection of such a structure is highly desired.

Acknowledgements

KD and MD acknowledge the financial support of Structural Funds in the Operational Programme Innovative Economy (IE OP) financed from the European Regional Development Fund Project Modern material technologies in aerospace industry, No. POIG.01.01.0200-015/0800. AK acknowledges the financial support of the National Science Centre (Poland) granted according the decision no. DEC-2011/03/N/ST8/06205. KD and MD would like to thank Lukasz Kornas, Artur Kurnyta, Patryk Kruszewski, Adam Latoszek and Michal Salacinski from AFIT for fruitful cooperation and discussions.

REFERENCES

[1] M. Sohn, X. Hu, J. Kim, L. Walker, Impact damage characterisation of carbon fibre/epoxy composites with multi-layer reinforcement, Composites Part B: Engineering 31 (8) (2000) 681–691.
[2] S.-X. Wang, L.-Z. Wu, L. Ma, Low-velocity impact and residual tensile strength analysis to carbon fiber composite laminates, Materials & Design 31 (1) (2010) 118–125.
[3] C. Poon, T. Benak, R. Gould, Assessment of impact damage in toughened resin composites, Theoretical and Applied Fracture Mechanics 13 (2) (1990) 81–97.
[4] C. Li, N. Hu, Y. Yin, H. Sekine, H. Fukunaga, Low-velocity impact-induced damage of continuous fiber-reinforced composite laminates. Part I. An FEM numerical model, Composites Part A: Applied Science and Manufacturing 33 (8) (2002) 1055–1062.
[5] J. Bieniaś, P. Jakubczak, B. Surowska, K. Dragan, Low-energy impact behaviour and damage characterization of carbon fibre reinforced polymer and aluminium hybrid laminates, Archives of Civil and Mechanical Engineering 15 (4) (2015) 925–932.
[6] R. Smith, L. Jones, B. Zeqiri, M. Hodnett, Ultrasonic C-scan standardisation for fibre-reinforced polymer composites: minimising the uncertainties in attenuation measurements, Insight 40 (1) (1998) 34–43.
[7] D. Roach, Industry Survey of Structural Health Monitoring Technology and Usage, Sandia National Laboratories, 2012.
[8] W. Staszewski, C. Boller, G.R. Tomlinson, Health Monitoring of Aerospace Structures: Smart Sensor Technologies and Signal Processing, John Wiley & Sons, 2004.
[9] V. Giurgiutiu, Structural Health Monitoring: With Piezoelectric Wafer Active Sensors, 2nd ed., Academic Press, 2014.
[10] T. Stepinski, T. Uhl, W. Staszewski, Advanced Structural Damage Detection: From Theory to Engineering Applications, John Wiley & Sons, 2013.
[11] Z. Su, L. Ye, Identification of Damage Using Lamb Waves: From Fundamentals to Applications, Springer, 2009.
[12] X. Zhao, H. Gao, G. Zhang, B. Ayhan, F. Yan, C. Kwan, J.L. Rose, Active health monitoring of an aircraft wing with embedded piezoelectric sensor/actuator network: I. Defect detection, localization and growth monitoring, Smart Materials and Structures 16 (4) (2007) 1208.
[13] X. Zhao, R.L. Royer, S.E. Owens, J.L. Rose, Ultrasonic lamb wave tomography in structural health monitoring, Smart Materials and Structures 20 (10) (2011) 105002.
[14] Z. Sharif-Khodaei, M. Aliabadi, Assessment of delay-and-sum algorithms for damage detection in aluminium and composite plates, Smart Materials and Structures 23 (7) (2014) 075007.
[15] T. Hay, R. Royer, H. Gao, X. Zhao, J. Rose, A comparison of embedded sensor lamb wave ultrasonic tomography approaches for material loss detection, Smart Materials and Structures 15 (4) (2006) 946.
[16] J.E. Michaels, Detection, localization and characterization of damage in plates with an in situ array of spatially distributed ultrasonic sensors, Smart Materials and Structures 17 (3) (2008) 035035.
[17] L. Qiu, S. Yuan, X. Zhang, Y. Wang, A time reversal focusing based impact imaging method and its evaluation on complex composite structures, Smart Materials and Structures 20 (10) (2011) 105014.
[18] I. Park, Y. Jun, U. Lee, Lamb wave mode decomposition for structural health monitoring, Wave Motion 51 (2) (2014) 335–347.
[19] Z. Su, L. Ye, Y. Lu, Guided Lamb Waves for Identification of Damage in Composite Structures: A Review, Journal of Sound and Vibration 295 (3) (2006) 753–780.
[20] Z. Su, X. Wang, Z. Chen, L. Ye, D. Wang, A built-in active sensor network for health monitoring of composite structures, Smart Materials and Structures 15 (6) (2006) 1939.
[21] H.-Y. Tang, C. Winkelmann, W. Lestari, V. La Saponara, Composite structural health monitoring through use of embedded PZT sensors, Journal of Intelligent Material Systems and Structures 22 (2011) 739.
[22] X.P. Qing, S.J. Beard, A. Kumar, T.K. Ooi, F.-K. Chang, Built-in sensor network for structural health monitoring of composite structure, Journal of Intelligent Material Systems and Structures 18 (1) (2007) 39–49.
[23] S. Mall, J. Coleman, Monotonic and fatigue loading behavior of quasi-isotropic graphite/epoxy laminate embedded with piezoelectric sensor, Smart Materials and Structures 7 (6) (1998) 822.
[24] K. Diamanti, C. Soutis, Structural health monitoring techniques for aircraft composite structures, Progress in Aerospace Sciences 46 (8) (2010) 342–352.
[25] C. Soutis, J.-B. Ihn, Design, analysis and structural health monitoring of bonded composite repair and substructure, in: C. Boller, F.-K. Chang, Y. Fujino (Eds.), Encyclopedia of Structural Health Monitoring, John Wiley & Sons, 2009 1923–1940.
[26] A. Vlot, GLARE – History of the Development of A New Aircraft Material, Kluwer Academic Publishers, 2001.